THE JOURNAL OF PHYSICAL CHEMISTRY A
A JOURNAL OF THE AMERICAN CHEMICAL SOCIETY

pubs.acs.org/JPCA

Article

Nitrogen Reduction to Ammonia on a Fe_{16} Nanocluster: A Computational Study of Catalysis

Gennady L. Gutsev,* Katharine M. Tibbetts, Lavrenty G. Gutsev, Sergey M. Aldoshin, and Bala R. Ramachandran

Cite This: *J. Phys. Chem. A* 2023, 127, 9052−9068

Read Online

ACCESS | Metrics & More | Article Recommendations | Supporting Information

ABSTRACT: The sequence of elementary steps leading to reductive ammonia formation from N_2 and H_2 catalyzed by a Fe_{16} cluster is studied using generalized gradient approximation density functional theory and an all-electron basis set of triple-ζ quality. The computational methods are validated by comparison to experimental data such as binding energies where possible. First, the associative and dissociative attachment of N_2 to Fe_{16} is considered, followed by exploration of the pathways leading to distal (Fe_{16}−N−NH_2) and enzymatic (NFe_{16}−NH_2) formation of an amino group. Next, the pathways leading to NH_3 formation in both distal and enzymatic cases are examined. Two mechanisms for NH_3 detachment have been discovered. An interesting peculiarity of the pathways is that they often proceed with total spin fluctuations, which are related to the rupture and formation of bonds on the surface of the catalyst over the course of the reactions. The reaction $Fe_{16} + N_2 + 2H_2 \rightarrow Fe_{16}NH + NH_3$ is found to be exothermic by 1.02 eV (93.8 kJ/mol).

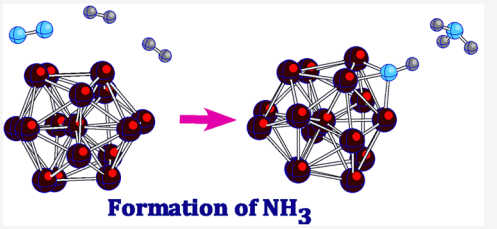

1. INTRODUCTION

Ammonia is an important component of many fertilizers and is widely used in many industrial applications. The use of ammonia in hydrogen storage[1] and as a carrier or supplier of hydrogen energy has attracted considerable attention in the scientific community.[2] A significant amount of effort has been spent on searching for more environmentally friendly and energy-efficient ways of reducing N_2 to NH_3, compared to the current industry standard, the Haber−Bosch process.[3] The latter has many drawbacks, such as its high energy demand (about 2% of global energy consumption), need for high temperatures of 400−500 °C and pressures of ∼200 atm, and large carbon footprint (∼1.0% to the global CO_2 emission). There are numerous approaches to reduce atmospheric nitrogen into ammonia[4,5] involving nitrogen fixation via nitrogenase complexes,[6,7] found in nitrogen-fixing bacteria. Other molecular complexes with active *nd*-metal centers[8,9] are also capable of nitrogen fixation. Presently, one of the more popular related areas of research is the electrochemical nitrogen reduction reaction (NRR) at ambient conditions,[10−13] including single-atom catalysis.[14] A relevant approach is presented by the photocatalytic ammonia synthesis[15] based on a redox conversion of dinitrogen and water into ammonia and dioxygen. However, the Haber−Bosch process, despite its high consumption of energy and high carbon dioxide emission, remains the only major industrial process of ammonia production estimated at about 150 million metric tons per year.

A quantum chemical study of N_2 activation by nitrogenase complexes appears to have been first attempted by Siegbahn et al.[16] by using several iron−sulfur clusters imitating the FeMo cofactor. More realistic models of nitrogenase were considered recently.[17] Heterogeneous catalytic formation of ammonia was modeled using FeN_3-embedded graphene,[18] Co_3Mo_3N surfaces,[19] oxynitrides,[20] and many others (see references in ref 20). Such studies are commonly based on several mechanistic models[21] of the NH_3 formation, which include

1. Distal: the NH_3 formation atop of an N atom attached to a catalyst surface.
2. Alternative: the NH_3 formation involving both N atoms of an N_2 dimer attached to a catalyst surface.
3. Enzymatic: the NH_3 formation on an N atom left after dissociation of an N_2 dimer on the catalyst surface.

The smallest catalyst for ammonia formation from N_2 is presented by a Ta_2^+ dimer. In the suggested process,[22] the N_2 dimer first dissociates to form a Ta_2N_2 rhombus and two NH_3 are formed after adding three H_2. Zhang et.al.[23] used a superalkaline cluster Ca_3B for the NH_3 formation and obtained Ca_3BNH_3 which is a congener of ammonia borate H_3NBH_3. In the recent research,[24] the clusters $Fe_{12}X$, where X is a 3d- or 4d-metal atom, were used for the ammonia formation via enzymatic-type pathways. Ammonia can also be formed from N_2 and H_2 on catalysts containing no *nd*-metal atoms.

Received: August 10, 2023
Revised: September 27, 2023
Published: October 19, 2023

https://doi.org/10.1021/acs.jpca.3c05426
J. Phys. Chem. A 2023, 127, 9052−9068

The present work is focused on a detailed computational study of the reaction pathways of NH_3 formation on a 16-atom nanoparticle of pure iron, Fe_{16}. To the best of our knowledge, this is the first computational study of this catalytic reaction on this form of Fe catalyst. As is well-known, the Haber−Bosch process uses an iron catalyst (with small amounts of additives) but not in nanoparticle form. The relevance of this study stems from the following considerations:

(a) The most active sites on a crystalline catalyst tend to be the defects, which deviate significantly from the periodic crystal geometry and may be closer to nanoparticle surfaces.
(b) The high surface energy of subnanometer metal clusters can contribute to increased catalytic activity. In our previous work,[25] the Fe_{16} nanoparticle was found to promote dissociative attachment of dinitrogen. That study also found that both N atoms and N_2 dimers prefer cluster surface sites and do not penetrate inside the cluster. The same cluster was also recently tested[26] as a catalyst for reactions of the CO_2 dissociation into separated atoms C and two O atoms on the surface of the cluster.
(c) Computationally, studying reactions of small molecules on small 3d-transition metal clusters makes it possible to use all-electron basis sets which can yield more precise descriptions—compared to plane wave methods that incorporate effective core potentials—of relevant electronic effects including the dependence of ground state energies on spin multiplicity which, the results of the present study show, play an important role in reaction energetics.
(d) It is now possible to synthesize size-selected subnanometer clusters of metals and metal oxides.[27] Therefore, the catalytic activity of ultrasmall nanoparticles is now amenable to be studied in detail in the laboratory.

It is hoped that insights into the pathways of ammonia formation on the Fe_{16} cluster will contribute to the design and optimization of improved catalysts for this extremely important reaction.

The geometrical structure of the ground-state Fe_{16} is less symmetric than that of the Fe_{13} cluster where all surface atoms have 5-fold coordination, while the surface atoms of Fe_{16} have both 5-fold and 6-fold coordination sites. The Fe_n clusters with n = 17−19 also have surface atoms with 4-fold coordination and possess less smooth surface than Fe_{16}.[28−30] Therefore, we have chosen Fe_{16} as a representative nanoparticle for $N_2 \rightarrow NH_3$ catalysis. First, we consider the attachment of N_2 to Fe_{16} associatively to form Fe_{16}−N_2, or dissociatively to produce two N atoms on the cluster surface. Adding H_2 in both cases of associative and dissociative attachment of N_2, pathways for the formation of −N−NH_2 (the distal case) and −NH_2 (the enzymatic case) are determined. By adding the second H_2 in both cases, we obtain NH_3 bound to an iron cluster (the −NH_3 type) or via an N atom (the −N−NH_3 type).

2. COMPUTATIONAL DETAILS

Our computations were carried out by using all-electron spin-polarized density functional theory (DFT) with the generalized gradient approximation (DFT-GGA) realized in the GAUSSIAN 16 program.[31] The well tested BPW91 method, where the exchange-correlation functional is composed of Becke's exchange[32] and Perdew−Wang's correlation,[33] and the 6-311+G* basis [Fe: (15s11p6d1f/10s7p4d1f),[34] N: (12s6p1d/5s4p1d) and H:(3s1s1s)[35] were used. Many assessments of various pure and hybrid DFT methods have shown the BPW91 method to be one of the most suitable methods for compounds containing transition metals.[36−39] In a recent work,[40] the BPW91 binding energies of nitrogen atoms to the Fe_n clusters in the range $4 \leq n \leq 10$ were found to match the experimental values[41] within the experimental accuracy bars. Computed in this work, the Fe_{16}−N bond strength of 5.19 eV is also in excellent agreement with the experimental value of[41] 5.18 ± 0.51 eV. An important advantage of the BPW91 method is its superior reproduction of antiferromagnetic states than that of several other widely used methods.[42]

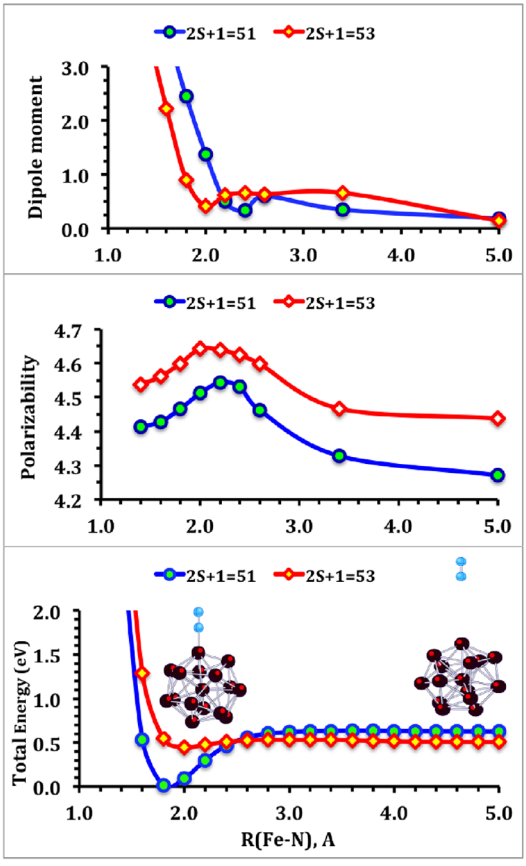

Figure 1. Total energy curves for the $Fe_{16}(2S + 1 = 53) + N_2(2S + 1 = 1)$ and $Fe_{16}(2S + 1 = 51) + N_2(2S + 1 = 1)$ systems as a function of the distance (in Å) between an N_2 dimer and a Fe atom on the surface of the Fe_{16} cluster. Zero energy corresponds to the total energy of the $Fe_{16}N_2(2S + 1 = 51)$ state (the lowest panel); the corresponding static electric polarizabilities per atom in $Å^3$ (the middle panel); and dipole moments in Debye (the top panel).

A typical reaction pathway consists of reactants followed by several transition states separated by local minima and terminates with the reaction products. After choosing a trial geometrical configuration, we perform computations by using the modified conjugate gradient algorithm developed by Schlegel[43] and subsequently improved by other authors[41] to reach a first-order transition state (TS) with one imaginary frequency. Next, we carry out intrinsic reaction coordinate (IRC)[44,45] computations to find two states which are connected via this TS. If one of these states is close in total energy to the previous state of the pathway and has a close geometric

https://doi.org/10.1021/acs.jpca.3c05426
J. Phys. Chem. A 2023, 127, 9052−9068

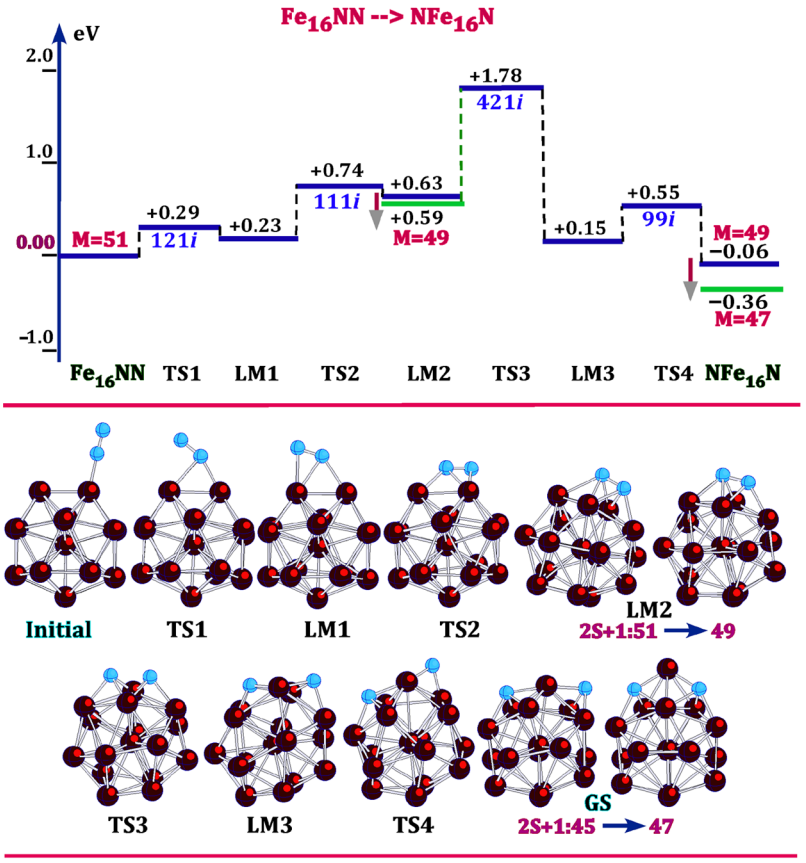

Figure 2. A pathway of N_2 dissociation on the ground-state Fe_{16} cluster to an $NFe_{16}N$ isomer when N_2 dimer was attached to a 5-fold coordinated Fe atom. The zero energy is below the sum of total energies (including the ZPVE) of Fe_{16} and N_2 by −0.46 eV. The top panel shows the imaginary frequencies obtained at transition states **TS*i***. The pathway contains two spin multiplicity changes on the local minima states. In this figure and those that follow, $M = 2S + 1$.

structure, we perform the geometry optimization of this state to make sure that the state found in the IRC procedure fits the state for which this TS search was performed. It should be noted that in the case of magnetic clusters several states may have close geometries but appreciably different total energies corresponding to several possible accommodations of the local total spin magnetic moments of magnetic atoms. This is quite a typical case for ferrimagnetic states but is less common for ferromagnetic states. In most cases, optimizations lead to the lowest energy states, but in some cases, additional effort is required to confirm that the IRC state and the lowest energy state with the same geometrical structures differ by only accommodations of local spins on iron atoms.

In the case of a magnetic catalyst, one should keep in mind that adsorption of atoms or molecules usually leads to changes in the total magnetic moment, whose predominant part in the case of iron clusters is due to the total spin magnetic moment.[46] For example, adding a single N atom to Fe_8 leads to a decrease in the total spin magnetic moment by 1.0 μ_B, from 24 μ_B to 23 μ_B, whereas deposition of two N atoms onto the Fe_{16} cluster surface results in reduction of the cluster total spin magnetic moment by 6 μ_B, from 52 μ_B to 46 μ_B.[25] In reactions catalyzed by Fe_{16}, the surface reactant compositions change which consequently results in changes of spin multiplicities (a spin multiplicity $2S + 1$ corresponds to the total spin magnetic moment of $2S$ μ_B) of the local minima states in reaction pathways.

According to a recent experimental study[47] of nitromethane by the time-resolved photoelectron spectroscopy, deexcitation of the first excited state occurs in 24 fs, while experiments using the ultrafast pump probe spectroscopy have shown deexcitations to occur within 110 ± 20 fs in the largest $Fe_{15}O_{16}$ cluster studied.[48] Generally, experimental demagnetization times are in the range 50−100 fs,[49] which is in line with the results of calculations by using spin-polarized time-dependent DFT for the bulk ferromagnets of Fe, Co, and Ni,[50] and with theoretical demagnetization lifetimes obtained in computations based on the spin−orbit coupling mechanisms.[51,52] Since vibrational excitation times are longer than the time scales of magnetic relaxations which are on the femtosecond scale, one should expect that magnetic relaxation times are much smaller than the times required to reach transition states. Therefore, magnetic relaxation can lead to states with smaller or larger spin multiplicities. For this reason, we always performed energy optimizations of local minima states obtained in the IRC procedure for several values of spin multiplicity in the vicinity of the spin multiplicity value of the preceding reaction step and identified the spin multiplicity of the lowest energy state. This procedure was repeated until the total energies of states with larger and smaller spin multiplicities became larger than total energies of their predecessors. The spin multiplicity of the lowest energy state found is regarded as the spin multiplicity of the next reaction step. Vibrational analysis was conducted on all stationary states to ensure that there were no imaginary frequencies. This process was continued until the final state, also optimized in the spin multiplicity, was reached.

https://doi.org/10.1021/acs.jpca.3c05426
J. Phys. Chem. A 2023, 127, 9052−9068

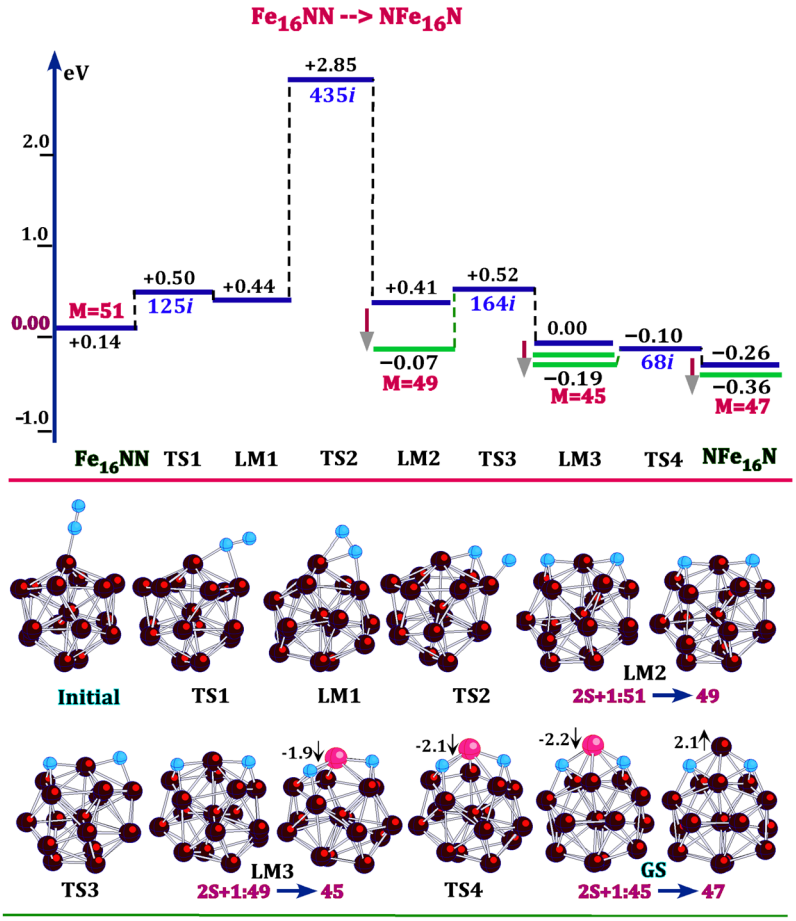

Figure 3. A pathway of N_2 dissociation on the ground-state Fe_{16} cluster to an $NFe_{16}N$ isomer when N_2 dimer was attached to a 6-fold coordinated Fe atom. The zero energy is the same as that in Figure 2. The top panel shows the imaginary frequencies obtained at the transition states TS*i*. The pathway contains three spin multiplicity changes on the local minima states.

The convergence threshold for total energy and the force threshold were set to 10^{-8} eV and 10^{-3} eV/Å, respectively. All energies in this work are obtained at 0 K. Occasionally, the force threshold was decreased to obtain a stronger convergence of optimized geometrical structures. Vibrational analysis was conducted on all stationary states to ensure there were no imaginary frequencies and on all transition states to verify that only one of the vibrational modes corresponded to an imaginary frequency. The energies of the stationary and transition states shown in the following section include zero-point energies. Local total spin magnetic moments on atoms were computed by using the natural atomic orbital populations (NAO) obtained from the NBO analysis.[53]

3. RESULTS AND DISCUSSION

This Section is organized as follows. First, in Section 3.1, we consider associative and dissociative attachments of N_2 to the ground-state Fe_{16} cluster. In Section 3.2, two pathways with the associative attachment of N_2 and two reaction pathways with the dissociative attachment of N_2 of the amino group formation are presented as well as a pathway for the dissociation of an H_2 dimer. In Section 3.3, the ammonia formation was modeled by adding the second H_2 to the amino groups. Both the distal Fe_{16}–N–NH_2 and enzymatic NFe_{16}–NH_2 cases were considered. Finally, the optimal combinations of the pathways leading to the ammonia production and the rate-limiting steps are discussed.

3.1. Attachment and Dissociation of N_2. According to a number of studies,[54,55] the preferred attachment of N_2 to *n*d-metal atoms and clusters is in the end-on position, which was experimentally confirmed for the $[Fe_n(N_2)_m]^+$ (n = 8–20) clusters[56,57] and mixed rhodium–iron clusters $[Rh_kFe_m]^+$ clusters.[58] Our optimizations have shown that the spin multiplicity $2S + 1 = 53$ of the ground-state Fe_{16} cluster decreases by two in the case of the $Fe_{16}N_2$ cluster with N_2 in the end-on position. To gain insight in the behavior of total energy curves of the $Fe_{16}N_2$ states with the spin multiplicities of $2S + 1 = 53$ and $2S + 1 = 51$ when an N_2 dimer is in its ground singlet state approaches to Fe_{16} from a large distance, relaxed potential energy scan computations with a step of 0.1 Å were performed. The total energy curves obtained are presented in Figure 1 together with the curves of the static electric polarizabilities and dipole moments of both states.

At large distances, the energy curve of $Fe_{16} + N_2$ with $2S + 1 = 51$ is higher than the energy curve with $2S + 1 = 53$ (the spin multiplicity of the isolated ground-state Fe_{16} cluster). Both energy curves intersect at a distance of ~2.5 Å, and the curve of the $2S + 1 = 51$ state drops below the curve with $2S + 1 = 53$ at smaller distances. Note that the orientation of N_2 toward the cluster remains the same as the dimer approaches the cluster. The total energy difference between the states of the Fe_{16} cluster with the spin multiplicities $2S + 1 = 51$ and $2S + 1 = 53$ is 0.12 eV, whereas the difference between the minima on the two energy curves equals 0.47 eV; i.e., the differences in total energies of the

https://doi.org/10.1021/acs.jpca.3c05426
J. Phys. Chem. A 2023, 127, 9052–9068

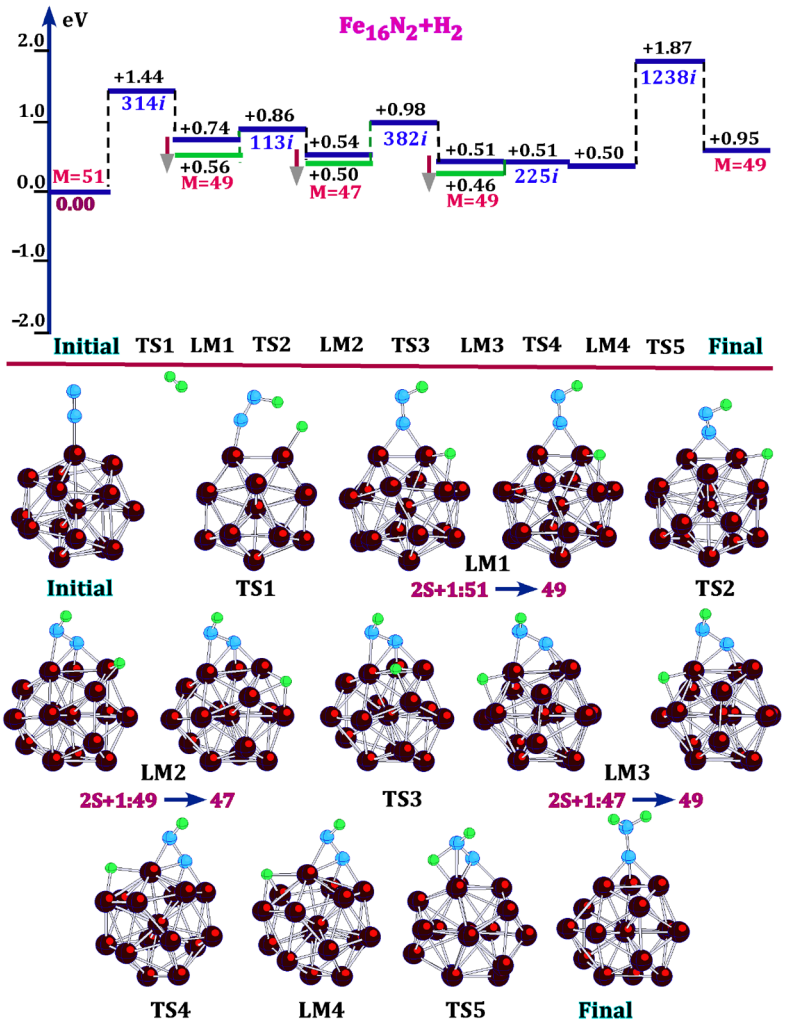

Figure 4. A pathway of the NH_2 formation when N_2 was attached associatively to a 5-fold coordinated Fe on the Fe_{16} cluster. The total energy shift with respect to the ground state of $Fe_{16} + N_2$ equals −0.46 eV plus the total energy of H_2, −31.67 eV, i.e., −32.13 eV (computed at the BPW91/6-311+G* level). The top panel presents the pathway energetics, while the geometrical presentation of the pathway is given below. The top panel also shows the imaginary frequencies obtained for the corresponding transition states **TS***i*, separated by the local minima **LM***i* on the potential energy surface. The pathway contains three spin multiplicity changes on the local minima states.

two $Fe_{16}N_2$ states are four times larger. The curves in Figure 1 show that there are no repulsive barriers for molecular N_2 adsorption. The binding energy of N_2 depends somewhat on the position of the Fe atom on the cluster surface to which N_2 is attached, and the adiabatic binding energies of N_2 to the 5-fold and 6-fold coordinated Fe atoms are 0.46 and 0.32 eV, respectively, and can be compared to the experimental binding energy of 0.29 ± 0.02 eV of N_2 on the Fe(110) surface.[59] The higher binding energy on Fe_{16} can be reasonably attributed to the higher surface energy of the nanocluster relative to the crystal surfaces. The local spin magnetic moment of the Fe atom to which N_2 is attached decreases by 1.1 μ_B due to an increase in the Fe β-3d4p electron population available for bonding. The bonding of N_2 to a *n*d-metal atom is understood[60] to be due to interactions of the metal atomic orbitals (AO) and the π^* orbital of N_2.

It can be seen in Figure 1 that the polarizability increases and reaches its maximum at $R(Fe_{16}–N_2) \sim 2.5$ Å, which corresponds to the vicinity of the intersection point of both energy curves, and it decreases when the $Fe_{16}–N_2$ distance decreases. That is, the movement of N_2 toward the Fe atom is due to polarization forces at large distances and the Fe−N_2 bond formation leads to a decrease in the polarizability. On the contrary, the dipole moments increase near the equilibrium bond distances.

No transition state was found for N_2 approaching the Fe_{16} cluster by using the gradient-based search, which is in line with the barrierless attachment of N_2 to a Fe atom in Figure 1. A search for pathways of N_2 dissociation was performed for two cases where N_2 attached to 5-fold and 6-fold coordinated iron atoms. The pathway with the lowest energy with respect to the sum of total energies (including the ZPVE) of Fe_{16} and N_2, shown in Figure 2 starts with N_2 attached to a five coordinate Fe atom and has three transition states (**TS**) before the N_2 bond cleavage occurs. The first **TS1** corresponds to N_2 tilting toward a neighboring Fe atom in such a way that the bottom N atom attaches to this Fe atom. The IRC procedure leads to a local minimum (**LM**) with the attachment of both N atoms to iron atoms. Optimizations of the **LM1** state in the spin multiplicity around $2S + 1 = 51$ did not result in any lower energy state. Therefore, the next step was started with $2S + 1 = 51$ and the **LM2** state relaxes to a state with $2S + 1 = 49$. The next step

https://doi.org/10.1021/acs.jpca.3c05426
J. Phys. Chem. A 2023, 127, 9052−9068

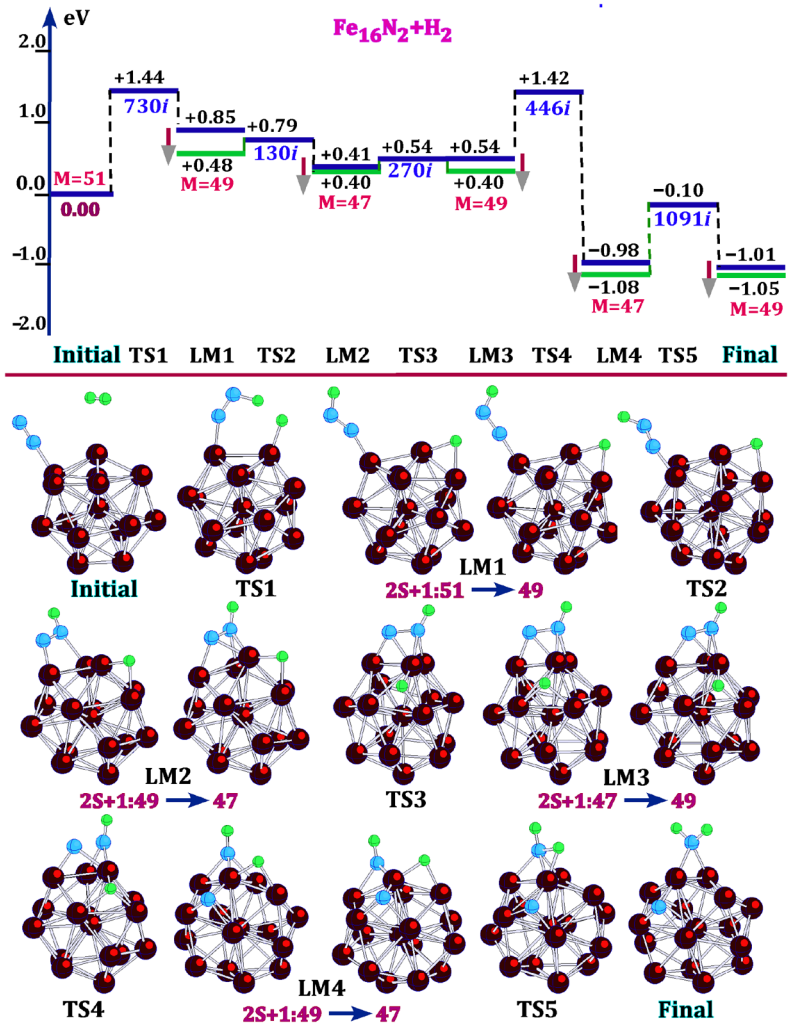

Figure 5. A pathway of NH_2 formation when N_2 was attached associatively to a 6-fold coordinated Fe on the Fe_{16} cluster. The top panel presents the pathway energetics while the geometrical presentation of the pathway is given below. The total energy shift with respect to the ground state of $Fe_{16} + N_2$ equals −0.38 eV plus the total energy of H_2, −31.67 eV (computed at the BPW91/6-311+G* level), i.e., −32.05 eV. The top panel also shows the imaginary frequencies obtained for the corresponding transition states **TS***i*, separated by the local minima **LM***i* on the potential energy surface. The spin multiplicity changes on four local minima states and the final state.

proceeds with $2S + 1 = 49$, and the final state of the pathway relaxes to the ground state of the $NFe_{16}N$ cluster.

The second pathway where an N_2 dimer is attached to a 6-fold coordinated Fe atom has two TSs preceding the N_2 collapse to two N atoms (see Figure 3) has the same first step as the previous pathway. The second **TS2** now corresponds to a cleavage of N_2 and is higher in energy by almost 1.0 eV than **TS2** in Figure 2. The IRC procedure leads to the final state, with N atoms attached to two Fe_3 faces on the Fe_{16} cluster surface. Optimizations of states with the geometrical structure of the final state and the spin multiplicities of 47, 49, 51, and 53 resulted in the lowest energy state with $2S + 1 = 49$. Two more steps are required to reach the ground-state $NFe_{16}N$ cluster. Dissociation energy of N_2 on the Fe_{16} cluster of 0.36 is somewhat less compared to the energies obtained for the N_2 dissociation on smaller iron clusters.[39]

3.2. Formation of Amino Groups. Since the Haber−Bosch process utilizes molecular hydrogen, we consider how NH_2 is formed by adding H_2 to Fe_{16}−N_2 in which the N_2 is attached associatively, and to N−Fe_{16}−N, in which the N_2 is attached dissociatively and the H_2 reacts with a single N atom on the cluster surface. First, we consider the case when N_2 is attached associatively to a Fe atom on the surface of the Fe_{16} cluster. Relative to the asymptotic ground states of $Fe_{16}N_2 + H_2$, the formation of the Fe_{16}−N−NH_2 lowest energy state with $2S + 1 = 51$ is energetically unfavorable by +1.36 eV. To gain insight into interactions of the top N atom with H_2, relaxed potential energy scan computations were performed for $Fe_{16}N_2 + H_2$ as a function of distance between this N atom and one of the H atoms. The results, shown in Figure S1 of the Supporting Information, indicate that the energy curve is repulsive and attachment of H_2 to $Fe_{16}N_2$ appears to follow a different mechanism. As will be seen below, the formation of Fe_{16}−N−NH_2 from Fe_{16}−N−N and H_2 is a complicated process that proceeds via multiple-step reaction pathways.

There are two scenarios of the NH_2 formation in the case of the associative attachment of N_2 to an iron cluster; namely, when the NH_2 formation involves the top N atom of the N_2 dimer (the so-called distal case) and when NH_2 sticks to the surface of the cluster (the so-called enzymic case). The pathway for −N−NH_2 formation is presented in Figure 4. The first transition state **TS1** corresponds to the stretching of the H−H bond with the

https://doi.org/10.1021/acs.jpca.3c05426
J. Phys. Chem. A 2023, 127, 9052−9068

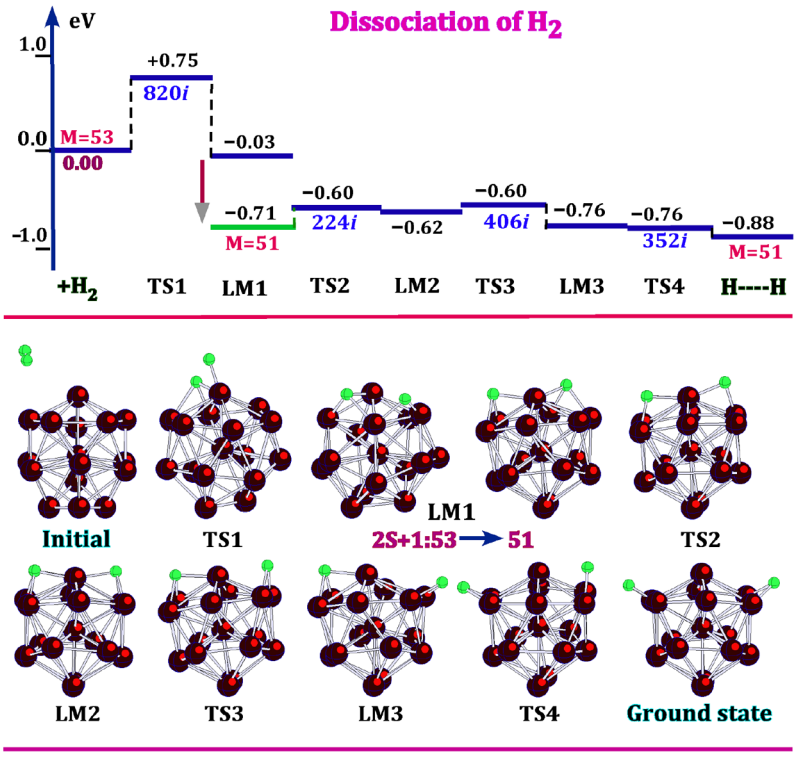

Figure 6. Dissociation of H_2 on the Fe_{16} cluster. The imaginary frequencies obtained for the corresponding transition states are also shown. This pathway contains four transition states and a single spin multiplicity change.

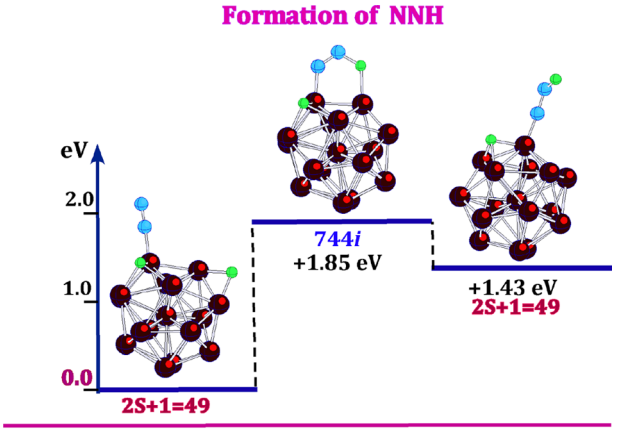

Figure 7. One-step formation of the −NNH group by lifting up an H atom from the cluster surface by a N_2 dimer attached associatively in one step. The complex number is the imaginary frequency obtained for the transition state.

subsequent formation of − N−NH and an H atom attached to an Fe−Fe edge (**LM1**). Optimizations of the **LM1** states in $2S + 1$ resulted in the multiplicity decreasing by two from 51 to 49. The **TS2** corresponds to the bending of −N−NH, and both N atoms become attached to iron atoms in the second local minimum state **LM2** which relaxes to a $2S + 1 = 47$ state. The **TS3** corresponds to an H atom displacement and the **LM3** has nearly the same geometrical structure as the **TS3** and relaxes to a state with a larger spin multiplicity. Thus, the spin relaxation can proceed in both decreasing and increasing directions of the total spin magnetic moment. The **TS4** corresponds to the H atom displacement into the Fe_3 face position in the **LM4** state without the $2S + 1$ change. In the final **TS5** state, H detaches from the face and attaches to an N atom. In the final state of the pathway, $-N-NH_2$ is formed on the top of a Fe_3 triangle. This state is above the dissociation limit $Fe_{16}N_2 + H_2$ by +0.95 eV, and the highest energy barrier of + 1.87 eV attained at **TS5** is related to the rupture of two Fe−H bonds without changing the spin multiplicity of the final state.

In the second scenario presented in Figure 5, the N−N bond breaks and both N atoms become attached to the cluster surface during the reaction process; this results in an amino group being formed on the cluster surface. Three pathways were found for this scenario; one of them with the lowest energy barrier is presented in Figure 5 and two others may be found in the Supporting Information. Comparing Figures 4 and 5, one can see that both **TS1** correspond to the stretch of the H_2 bond, but the first local minima of LM1 are different. At the second step, the −N−NH group changes its supporting Fe atom in the **TS2**, and the second N atom attaches to the Fe atom which previously supported the −N−NH group in the **LM2** state which relaxes to a state with the spin multiplicity $2S + 1 = 47$ where the −NNH group tilts toward a Fe atom and both N atoms become bound to the third Fe atom. The third transition state **TS3** corresponds to the single H atom migration to a Fe_3 face which leads to an increase of the spin multiplicity by two of the **LM3** state. Separation of nitrogen atoms occurs in **TS4**, where the single H atom moves to an Fe_2 edge position that leads to reducing the spin multiplicity of the **LM4** state by two.

The single H atom becomes attached to both Fe and N atoms in **TS5**, and the final state is formed by breaking the Fe−H bond which leaves the amino group NH_2 in the bridge position between two Fe atoms. Such position was found to be preferred in the DFT study of adsorption of NH_2 on the Fe(110) surface.[61] The adsorption energy E_{ads} is computed in this work according to the formula:

https://doi.org/10.1021/acs.jpca.3c05426
J. Phys. Chem. A 2023, 127, 9052−9068

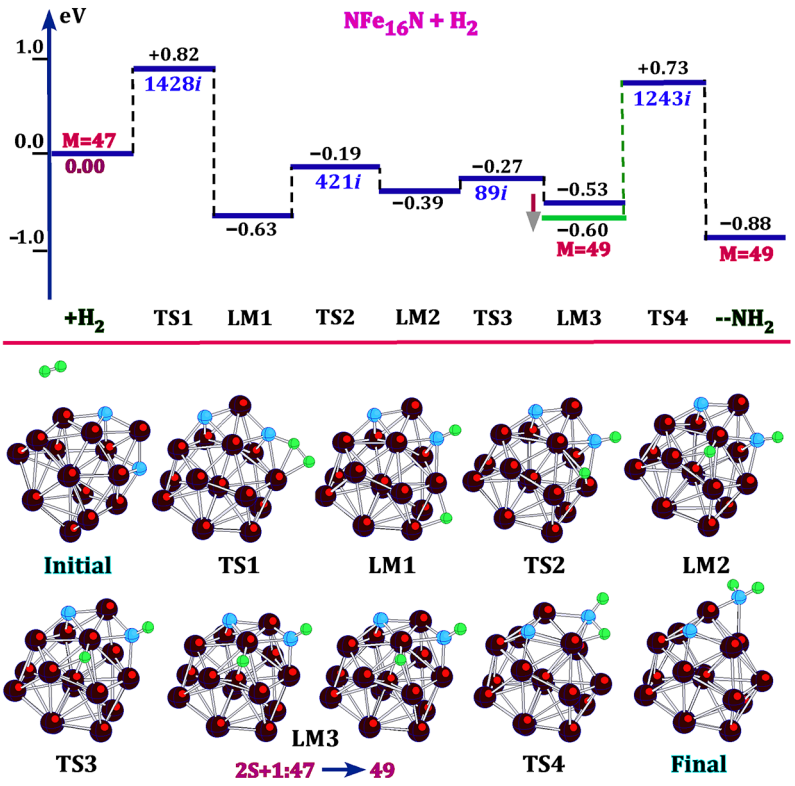

Figure 8. A pathway the NH_2 formation on the ground-state $NFe_{16}N$ cluster, when N_2H is attached to Fe_{16} dissociatively. The total energy shift with respect to the ground state of Fe_{16} + N_2 equals −0.82 eV + the total energy of H_2, −31.67 eV, i.e., −32.49 eV (computed at the BPW91/6-311+G* level). The top panel presents the pathway energetics, while the geometrical presentation is given below. The complex numbers in the top panel are the imaginary frequencies obtained for the corresponding transition states **TS***i*, separated by the local minima **LM***i* on the potential energy surface. The pathway contains a spin-multiplicity change on the **LM3** state.

$$E_{ads}(Fe_{16}N{-}NH_2) = [E_{el} + E_{zp}]_{Fe_{16}N} + [E_{el} + E_{zp}]_{NH_2} - [E_{el} + E_{zp}]_{Fe_{16}N_2H_2} \quad (1)$$

where E_{el} is the Born−Oppenheimer energy and E_{zp} is the zero-point vibrational energy. The value obtained, E_{ads} = 3.46 eV, is in reasonable agreement with the value range of 2.97−3.03 eV obtained for the NH_2 attachment to the Fe(110) surface, especially if one accounts for the higher surface energy of a nanocluster compared to a crystal surface. Experimental data were also obtained[62] for binding energies of ND_2 to a series of the Fe_n^+ cations, and the average binding energy[63] of 3.2 ± 0.2 eV is in line with our value for the NH_2 binding energy.

Two more pathways of amino group formation are presented in Figures S2 and S3 of the Supporting Information. The largest barrier heights in these figures are 1.91 and 2.29 eV, respectively, whereas the largest barrier heights in Figures 4 and 5 are 1.87 and 1.44 eV, respectively.

It is not necessary that H_2 interacts directly with N or N_2; H_2 can first dissociate, and H atoms formed could approach an N atom or an N_2 dimer due to the high mobility of H atoms. Dissociation of H_2 on Fe_{16} cluster proceeds in one step and the next three steps are required to reach the ground state of the $Fe_{16}H_2$ cluster. As can be seen in Figure 6, the barrier heights for the H movement over Fe−Fe edges are ∼0.1 eV.

Hydrogen atoms can approach an N_2 dimer attached associatively to the Fe_{16} cluster, and a −NNH group can be formed in one step (see Figure 7) similar to the −NNH group formation shown in Figure 5, and the formation of amino group can proceed in a similar way.

In the case of dissociative attachment of N_2 to Fe_{16}, there are two N atoms separated by a Fe atom, and NH_2 is formed by adding H_2 to one of the nitrogen atoms. We found two pathways leading to the formation of NH_2 with all ferromagnetic local minima states and with intermediate ferrimagnetic states where one local total spin magnetic moment flips, i.e., couples antiparallel to the local total spin magnetic moments of all other Fe atoms. The first scenario is presented in Figure 8, where the first transition state TS1 corresponds to the sharing of the H_2 dimer between the Fe and N atoms. After the H−H bond rupture in the LM1 state, one H atom attaches to the N atom, and NH is tetracoordinate. The next two steps are required for the single H atom movement toward NH; the LM3 state relaxes in the spin multiplicity, and NH becomes tricoordinate. Next, the migrant H atom shares the same Fe atom with NH in the TS4, and the IRC procedure delivers the final state with NH_2 in a bridge position. This process is exothermic, with the highest energy barrier being quite moderate: + 0.82 eV.

In the second scenario presented in Figure 9, an H_2 dimer attaches to the Fe atom connecting two nitrogen atoms practically without an energy barrier. The local minimum **LM1** obtained with the initial spin multiplicity of 47 relaxes to 2*S* + 1 = 45 accompanied by the spin flip on the Fe atom which is bonded to two N atoms and H_2 in the side-on position. The local total spin magnetic moment computed as the difference of excess spin densities of this Fe atom is −2.3 μ_B and is coupled antiparallel to the local total spin magnetic moments of all other Fe atoms. The second transition state **TS2** has the geometrical

https://doi.org/10.1021/acs.jpca.3c05426
J. Phys. Chem. A 2023, 127, 9052−9068

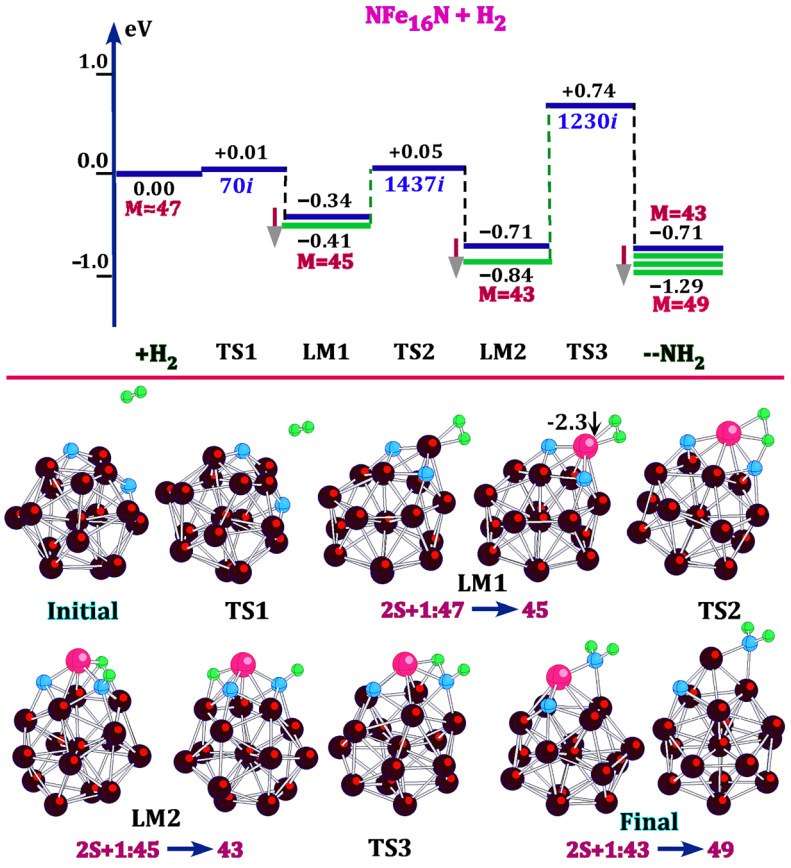

Figure 9. Second pathway the NH_2 formation on the ground-state $NFe_{16}N$ cluster, which proceed via ferrimagnetic intermediate states. A pink Fe atom has a local total spin magnetic moment coupled antiferromagnetically to the rest of the Fe atoms. The zero energy is the same as Figure 8 The top panel presents the pathway energetics while the geometrical presentation is given below. The complex numbers in the top panel are the imaginary frequencies obtained for the corresponding transition states **TS***i*, separated by the local minima **LM***i* on the potential energy surface. The pathway contains a spin-multiplicity change on the **LM3** state.

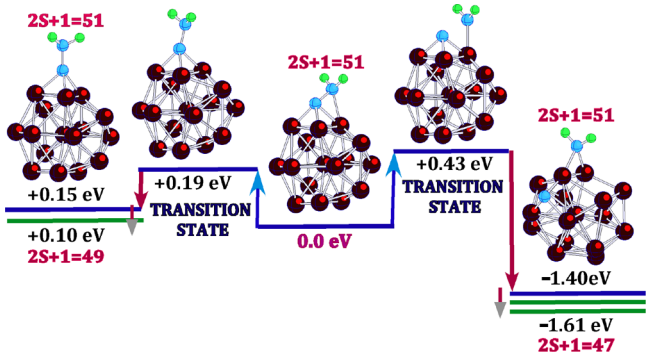

Figure 10. A switch mechanism between the distal and enzymatic attachments of NH_2.

structure similar to that of the first transition state **TS1** in Figure 8, where H_2 is bound to both Fe and N atoms in a fan-like type. But the H−H bond rupture in the **LM2** state leaves the second H atom in the vicinity of NH and no H migration is required. This H atom moves to NH in the **TS3** state, and the Fe−H breakage results in a magnetically excited final state. The spin relaxation leads to an increase in the multiplicity from 43 to 49 and the final state becomes ferromagnetic. This pathway has two spin multiplicity decreases on the local minima states and multiple changes in the spin multiplicity on the final state from $2S + 1 = 43$ to $2S + 1 = 49$. The largest energy barrier of this pathway has a moderate height of +0.87 eV.

As can be seen in Figure S4 of the Supporting Information where the lowest energy isomers of $Fe_{16}N_2H_2$ with different geometrical structures are presented, the global minimum state has the structure with dissociative attachment of both H_2 and N_2. Dissociation of both dimers on the cluster surface leads to a sharp decrease in the spin multiplicity of the initial Fe_{16} cluster, from $2S + 1 = 53$ to $2S + 1 = 45$. It is remarkable that N and H atoms share three adjacent Fe vertices, thus forming a seven-atom chain. The lowest energy isomer with NH_2 attached to a Fe−Fe edge is higher in energy by only 0.29 eV, followed by an isomer with two NH dimers sharing the same Fe atom. The higher energy isomers possess geometric strictures corresponding to various distributions of H and N atoms over the Fe_{16} cluster surface.

The distal and enzymatic positions of NH_2 can be transformed (switched) from one another via two transition states as shown in Figure 10. The middle reference state is similar to the **LM4** state in Figures S1 and S2 of the Supporting Information. Depending on the position of a single N atom, the spin multiplicity of the lowest energy state of NFe_{16}−NH_2 can be $2S + 1 = 47$ or $2S + 1 = 49$ with quite a small energy difference between them. One can observe in Figure 8 that a transition to the distal −N−NH_2 position is endothermic by 0.10 eV, whereas it is exothermic by −1.61 eV in the enzymatic case and the energy difference between the resulting states is 1.71 eV.

https://doi.org/10.1021/acs.jpca.3c05426
J. Phys. Chem. A 2023, 127, 9052−9068

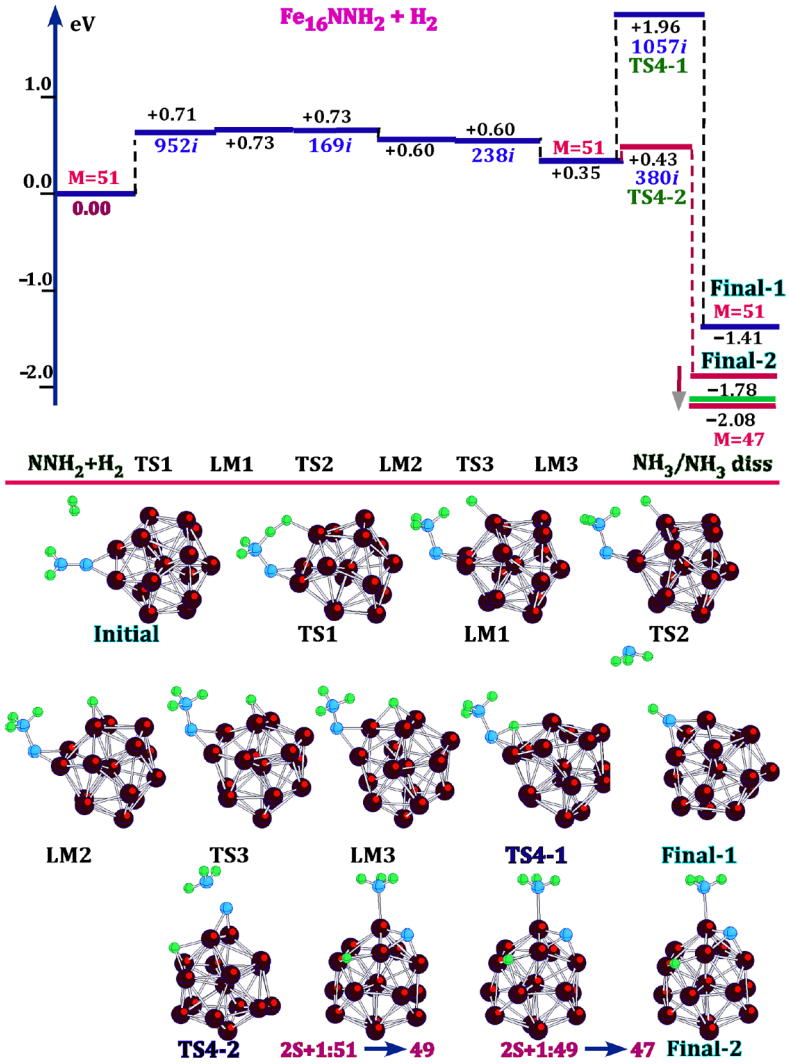

Figure 11. A pathway of the NH_3 formation when an N−NH_2 group is attached to the Fe_{16} cluster. The total energy shift with respect to the ground state of Fe_{16} + N_2 + H_2 equals +0.39 eV + the total energy of H_2, −31.67 eV, i.e., −31.28 eV (computed at the BPW91/6-311+G* level). The top panel presents the pathway energetics, while the geometries are presented below. The complex numbers in the top panel are the imaginary frequencies obtained for the corresponding transition states **TS***i*, separated by the local minima **LM***i* on the potential energy surface. The pathway splits in the end to **TS4-1** and **TS4-2**, one of which leads to the detachment of NH_3, and another one results in NH_3 directly attached to the cluster.

3.3. Formation of NH_3. Adding an H_2 dimer to the final states of $Fe_{16}N_2H_2$ obtained in the previous section, the pathways leading to the formation of NH_3 were obtained for both the distal and enzymatic cases. First, we consider a pathway that starts with adding H_2 to the distal −Fe_2−N−NH_2 geometrical configuration and the spin multiplicity $2S + 1 = 51$, which is the spin multiplicity of the lowest energy state of $Fe_{16}N_2H_2$ with this geometry. The initial state with the edge attachment, shown in Figure 11, corresponds to a local minimum and can be obtained from the final state in Figure 4 by breaking one Fe−N bond in the −Fe_3−N−NH_2 configuration. The energy difference between the states with two- and three-coordinate attachment of NNH_2 is only 0.06 eV. The pathway shown in Figure 11 consists of four steps with two final states, one of which corresponds to NH_3 detachment (**Final-1**) and the other one corresponds to the formation of NH_3 attached to a single Fe atom on the cluster surface (**Final-2**). All states of the former pathway have the same spin multiplicity $2S + 1 = 51$, while the detachment of NH_3 leaves $Fe_{16}NH$ in a state with the spin multiplicity of $2S + 1 = 47$.

The first transition state **TS1** corresponds to bonding of a stretched H_2 dimer to a Fe atom, the distal N atom followed the H−H bond rupture in the first local minimum state, and a distal NH_3 is formed in one step. It requires only 0.02 eV to reach the second transition state **TS2** which connects **LM1** with **LM2** where the single H atom attaches to the second Fe atom to form a Fe−H−Fe bridge. The next transition state corresponds to the tilting of the H atom toward the N−NH_3 group and the H atom becomes three-coordinate in **LM3**. In **TS4-1**, the H atom moves toward the N atom and the formation of a NH group leads to detachment of NH_3 in the final state. This detachment proceeds via the formation of metastable NH_4 when the H atom pushes NH_3 up. However, **TS4-1** corresponds to a high energy barrier of +1.61 eV with respect to the **LM3** state, whereas there is the second transition state **TS4-2**, where the N−NH_3 bond is stretched, which is higher in energy than the **LM3** state by only 0.08 eV, where the N−NH_3 bond is stretched. The next local

https://doi.org/10.1021/acs.jpca.3c05426
J. Phys. Chem. A 2023, 127, 9052−9068

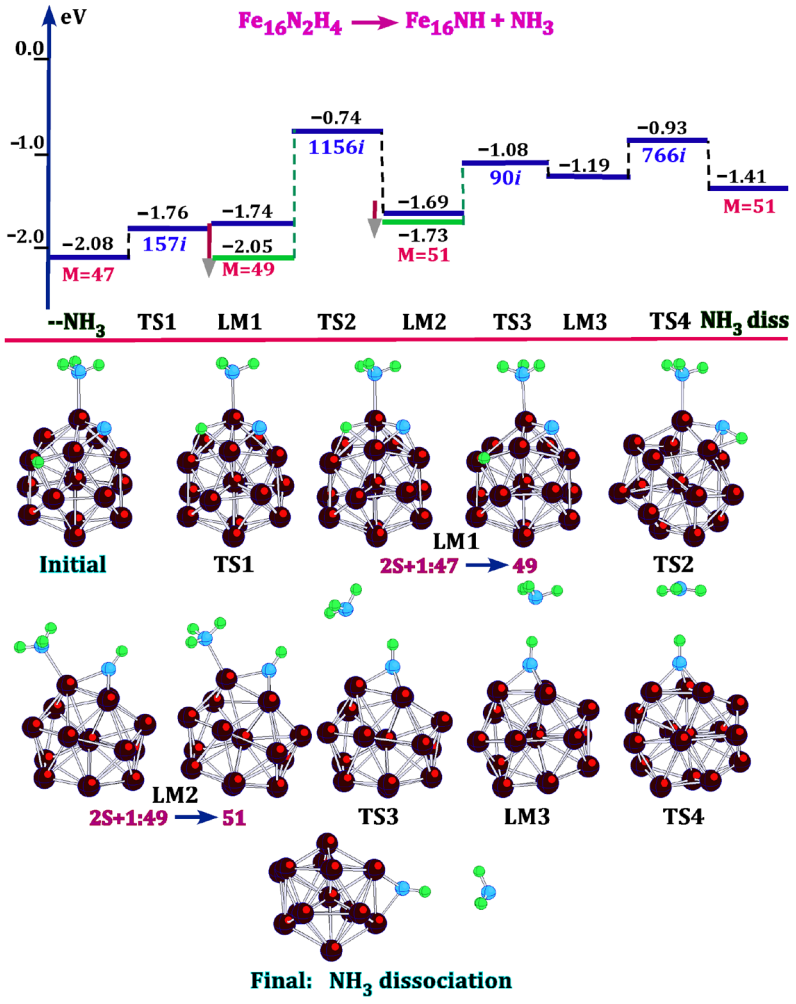

Figure 12. A pathway leading to the detachment of NH_3 for the second pathway in the previous case. The top panel presents the pathway energetics while the geometries are presented below. The top panel also shows the imaginary frequencies obtained for the corresponding transition states **TS***i*, separated by the local minima **LM***i* on the potential energy surface. The pathway has two spin flips, leading to an increase in the spin multiplicity from 47 to 51. The dissociation energies of ammonia with respect to the initial and LM2 states are 0.67 and 0.32 eV, respectively.

minimum state has a geometrical configuration where NH_3 is attached to a single Fe atom, and the second N atom is three-coordinate. The double relaxation from the spin multiplicity $2S + 1 = 51$ to $2S + 1 = 47$ results in the second final state of this pathway.

A pathway leading to the detachment of NH_3 from the second **Final-2** state in Figure 11 is shown in Figure 12. Here, the first transition state **TS1** corresponds to approaching the single H atom to the single N atom and **TS2** serves as a connector of H to N. Next, NH tilts toward NH_3 to form a temporary H−NH_3 complex. In the local minimum state **LM3**, the NH dimer is three-coordinate and NH_3 is weakly attached to the top H atom of the NH group. The flat geometry of NH_3 is realized in **TS4** and the inversion of all three H atoms leads to the repulsion of NH_3 in an arrow-type way. This detachment is different from that in Figure 11 by an additional transition state required for the inversion of the NH_3 geometrical structure. Note that the spin multiplicity increases in this pathway from $2S + 1 = 47$ to $2S + 1 = 51$.

A pathway which presents a sort of a hybrid of the two pathways in Figures 11 and 12 and leads to the NH_3 detachment is shown in Figure 13. The initial state in this case was formed as a result of the first H_2 dissociation which left one H atom on the top of the adsorbed N_2 dimer. Addition of the second H_2 leads to the first transition state **TS1** followed by the local minimum **LM1** where the distal NH_2 is formed. This formation leads to a decrease in the spin multiplicity due to the attachment of the second H atom to the cluster surface in a tricoordinate position. Next, this hydrogen atom is shared between the top N atom and a surface Fe atom in **TS2** and a distal NH_3 formed in **LM2** accompanied by an increase in the spin multiplicity due to the loss of the H atom on the cluster surface. The transition state **TS3** is followed by the local minimum **LM3**, which is lower in total energy than **LM2** by 2.60 eV. This gain in energy is due to the formation of an additional bond between the bottom N atom and a surface Fe atom and the formation of a single bond Fe−NH_3 which results in a decrease in the spin multiplicity from $2S + 1 = 51$ to $2S + 1 = 47$. The H and N atoms approach each other in **TS4**, and the NH formation in **LM4** is accompanied by an increase in the spin multiplicity due to the removal of the H atom from the cluster surface. The **LM4** geometrical structure is similar to the one of the **LM2** state in Figure 12, but the corresponding states have different spin multiplicities, which can be attributed to the different positions of NH and NH_3 on the Fe_{16} surface. The transition state **TS5** is similar to **TS3** in Figure 12, and the dissociation proceeds in much the same way (the

https://doi.org/10.1021/acs.jpca.3c05426
J. Phys. Chem. A 2023, 127, 9052−9068

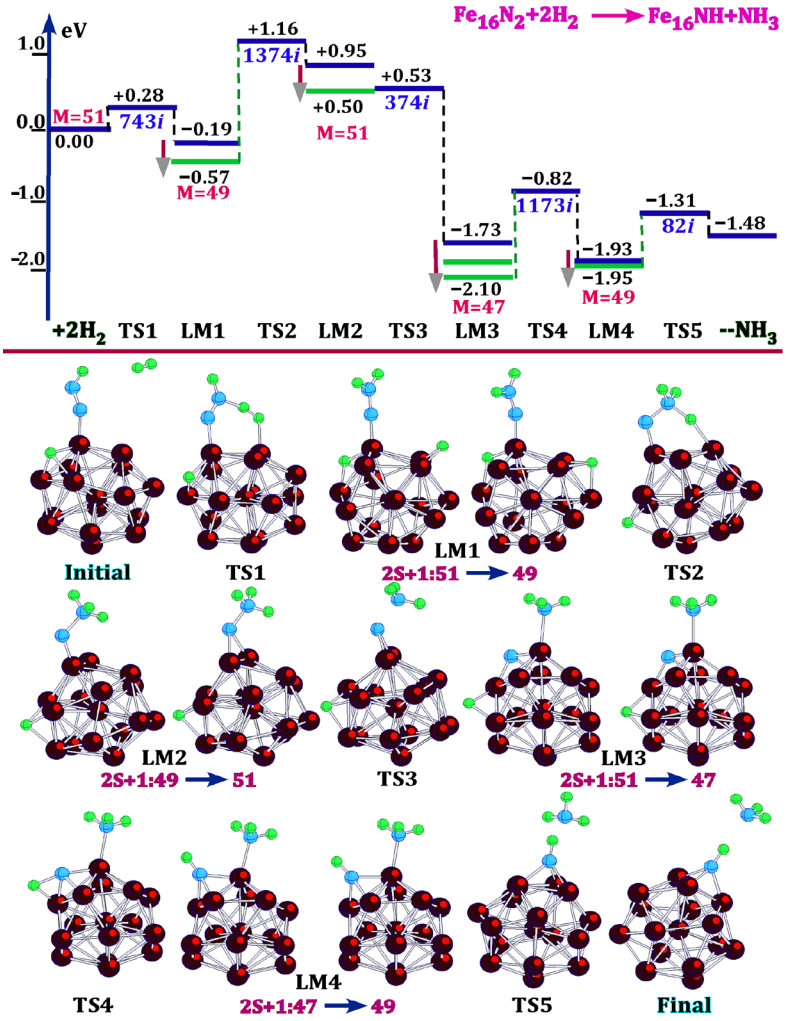

Figure 13. A pathway of NH_3 formation and detachment in the case when an NNH group is formed after dissociation of H_2 on the $Fe_{16}N_2$ cluster. The total energy shift with respect to the ground state of Fe_{16} + N_2 + H_2 equals +0.47 eV + the total energy of H_2, −31.67 eV, i.e., −31.20 eV (computed at the BPW91/6-311+G* level). The top panel presents the pathway energetics while the geometries are presented below. The top panel also shows the imaginary frequencies obtained for the corresponding transition states **TS***i*, separated by the local minima **LM***i* on the potential energy surface. There are five spin flips in this pathway.

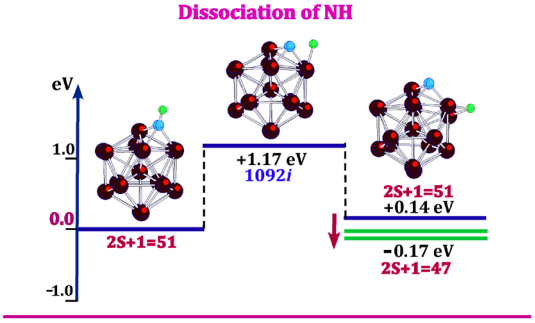

Figure 14. Dissociation of NH on the Fe_{16} cluster. The complex number is the imaginary frequency of the transition state. The dissociation pathway contains a single transition state.

transition state corresponding to the NH_3 planarization is omitted).

The NH dimer was left on the Fe_{16} cluster after the ammonia detachment. can dissociate in a one-step process, as is shown in Figure 14. In the reverse process, NH can be formed from N and H with the appropriate changing spin multiplicities. Dissociation of NH leads to the formation of new chemical bonds of the H atom with two Fe atoms accompanied by the corresponding lowering in the spin multiplicity. The opposite process leads to an increase in the spin multiplicity.

The pathway of the NH_3 formation involving an $NFe_{16}NH_2$ cluster displayed in Figure 5 as the final state is shown in Figure 15. The first transition state **TS1** corresponds to the attachment of an H_2 dimer to a Fe atom which dissociates to form the **LM1** state. The H_2 dissociation results in the formation of multiple bonds between two H atoms and the surface Fe atoms accompanied by the triple spin multiplicity relaxation. In **TS2**, an H atom becomes two-coordinate on the way toward the amino group, and the decrease in the number of bonds leads to an increase in the spin multiplicity in the **LM2** state. In **TS3**, the H atom becomes singly bonded and forms a bond with one of the Fe atoms supporting the amino group. The H atom attaches to the N atom of the amino group in **TS4**, and ammonia formed in the final state of the pathway. Detachment of NH_3 may proceed in the way shown in Figure 12. A pathway where H_2 is attached to another Fe atom has a larger barrier height and is presented in Figure S5 of the Supporting Information.

https://doi.org/10.1021/acs.jpca.3c05426
J. Phys. Chem. A 2023, 127, 9052−9068

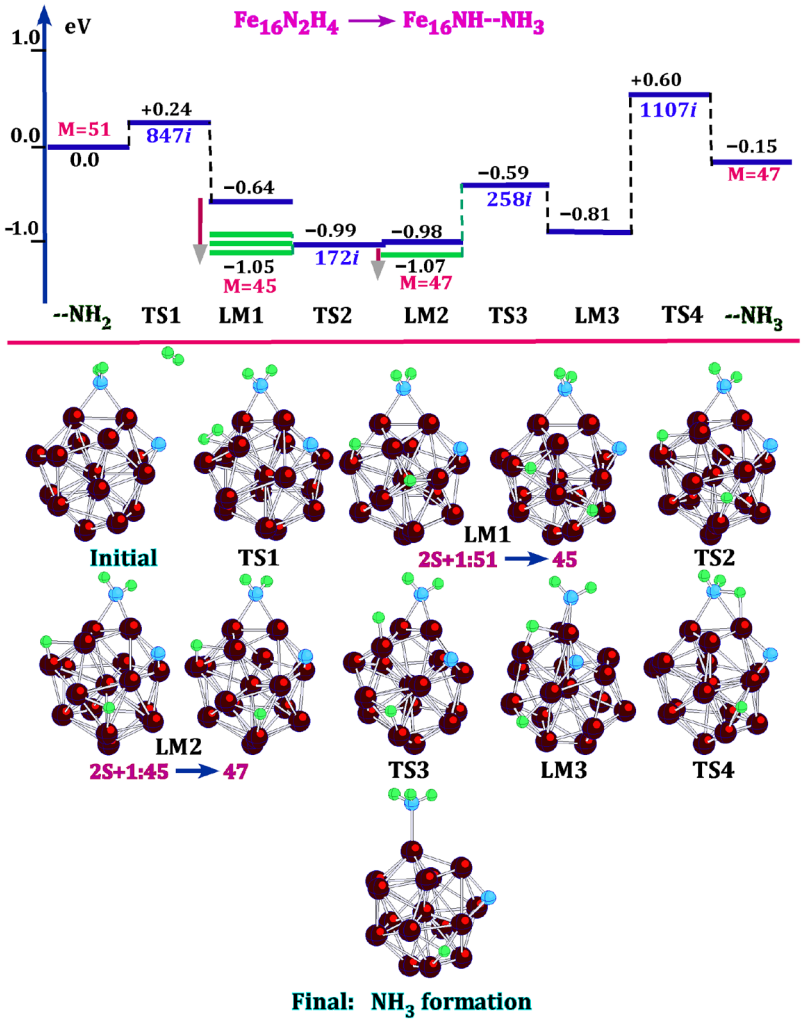

Figure 15. A pathway of NH_3 formation when an NH_2 group is attached to the Fe_{16} cluster. The total energy shift with respect to the ground state of $Fe_{16} + N_2 + H_2$ equals −1.43 eV + the total energy of H_2, −31.67 = −33.12 eV (computed at the BPW91/6-311+G* level. The top panel presents the pathway energetics while the geometries are presented below. The top panel also shows the imaginary frequencies obtained for the corresponding transition states TS*i*, separated by the local minima LM*i* on the potential energy surface. There are four spin flips in this pathway.

In addition to the **TS5** state leading to detachment of NH_3 in Figure 13, there is a transition state leading to the release of H_2. Two reaction steps involving both transition states from the initial state **LM4** in Figure 13 are displayed in Figure 16. As may be seen, the transition state that corresponds to the H_2 detachment is higher by 1.92 eV relative to the initial state (**LM4** in Figure 13) and is higher by 1.28 eV than the transition state corresponding to the NH_3 detachment. The energy of the initial state in Figure 16 is below the sum of energies of reactants $Fe_{16} + N_2 + 2H_2$ by −1.48 eV, which means that the barrier for NH_3 detachment in Figure 13 is −0.84 eV, while that for H_2 detachment is above by +0.44 eV. Therefore, the major channel should correspond to the formation of ammonia while the second channel produces H_2 which can repeatably be used in the next cycle of the NH_3 production.

The relative order of $Fe_{16}N_2H_4$ isomers found in a separate search for isomers and obtained as local minima states can be seen in Figure 17. The global minimum state has a geometrical structure with dissociated N_2 and two H_2. The gain in total energy due to this dissociation computed as

$$E_{diss}(Fe_{16}{-}2N{-}4H) = [E_{el} + E_{zp}]_{Fe_{16}} + [E_{el} + E_{zp}]_{N_2} + 2[E_{el} + E_{zp}]_{H_2} - [E_{el} + E_{zp}]_{Fe_{16}N_2H_4} \quad (2)$$

(notations are explained under eq 1) equals 2.98 eV. The next seven isomers containing an NH_2 group are higher in energy by 0.10−0.77 eV and are followed by a group of isomers with atop NH_3. The adiabatic binding energy of NH_3 can be computed as the difference in total energy between the isomer at +1.18 in Figure 17 and the sum of total energies of $Fe_{16}NH$ and NH_3 by using modified eq 2. The value of +0.78 eV obtained in this way can be compared with the experimental values of 0.88 ± 0.02 eV obtained[64] for the Fe_n clusters (n = 19, 23, 26, 29, 32, and 34), where no size dependence of the NH_3 binding energy was observed. Our value also compares well with previously found values of +0.91 eV from DFT computations[65] for $Fe_{13}(NH_3)_2$ and +0.83 eV computed[66] for the atop position of NH_3 on the Fe(110) surface. However, the detachment energy of NH_3 depends on the disposition of atoms N and H relative to each other. The smallest energy of the NH_3 detachment with respect to the isomer at 1.63 eV in Figure 17 is only 0.33 eV.

https://doi.org/10.1021/acs.jpca.3c05426
J. Phys. Chem. A 2023, 127, 9052−9068

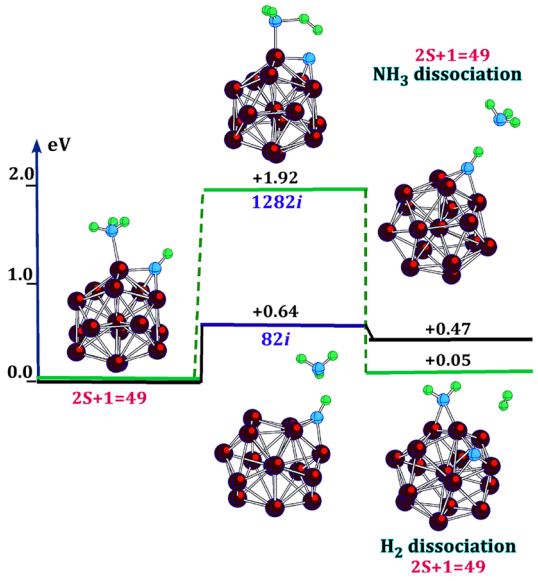

Figure 16. Formation of either H_2 or NH_3 when an NH_3 group is neighbored by an NH group. The top panel also shows the imaginary frequencies obtained for the corresponding transition states. The initial state at 0.0 eV is below the sum of total energies of Fe_{16}, N_2, and two H_2 by 1.48 eV.

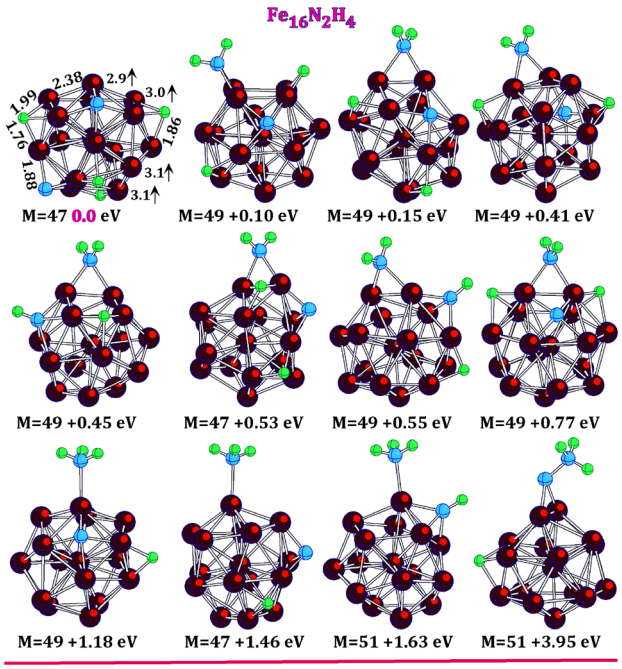

Figure 17. Lowest energy states for different topologies of $Fe_{16}N_2H_4$ isomers. Interatomic distances and local total spin magnetic moments on iron atoms are shown for the global minima state whose total energy is the reference one. The interatomic distances are in Å, the local total spin magnetic moments (their directions are shown by arrows) are in Bohr magneton, and M denotes the spin multiplicity $2S + 1$.

4. CONCLUSIONS

In the present work, we considered the reaction pathways leading first to the formation of an amino group, followed by the formation of ammonia. Our simulations were performed by using all-electron spin-polarized density functional theory with the generalized gradient approximation (DFT-GGA) and the basis set of triple-ζ quality. The reliability of this approach is confirmed by the close agreement between computed and experimental values of binding energies of an N atom and NH_3 to Fe_{16}. An N_2 dimer attaches atop a single Fe atom with a quite small binding energy of 0.3−0.5 eV; however, this attachment leads to a decrease in the local total spin moment of this Fe atom which means that the β-electron density, responsible for chemical bonding in iron clusters,[25] increases, and the spin multiplicity of Fe_{16}−NN decreases to $2S + 1 = 51$ with respect to the spin multiplicity of $2S + 1 = 53$ of noninteracting $Fe_{16}(2S + 1 = 53) + N_2$(singlet). The barrier height for the dissociation of N_2 appears to depend on the coordination number of the Fe atom to which N_2 is attached. There are many different scenarios for NH_3 formation beginning with both the associatively and dissociatively attached N_2. Compound pathways of the dinitrogen reduction to ammonia formation can be constructed using pathways shown in Figures 2−15.

The compound pathway with the lowest barrier heights can be obtained by a combination of the two pathways shown in Figure 5 (the NH_2 formation) and Figure 15 (the NH_3 formation). This is shown in Figure S6, where a common energy axis relative to $Fe_{16} + N_2 + 2H_2$ is adopted. The highest barrier height along this path, relative to the reference energy, is **1.07** eV corresponding to the TS1 of Figure 5. This compound pathway begins with N_2 associatively attached to Fe_{16}.

Another compound pathway starting with the dissociated adsorption of N_2 can be obtained by combining the reaction pathways shown in Figure 2, Figure 8, and Figure 15, as shown in Figure S7. Relative to the same zero energy as in Figure S6, the highest barrier height on this pathway is **1.33** eV corresponding to TS3 of Figure 2. The rate-limiting step in this case is the N_2 dissociation (TS3), which was also considered by Ertl[67,68] as the rate-limiting step in the ammonia production catalyzed by Fe (110), (100), and (111) single crystal surfaces.

Figure S8 shows the compound pathway beginning with dissociation of H_2 on Fe_{16} (Figure 6) followed by associative adsorption of N_2, passing through the intermediate H−Fe_{16}-NNH (Figure 7), culminating in the formation of ammonia (Figure 13) and involves the highest barrier of **1.68** eV corresponding to the TS state of Figure 13.

One more compound pathway that does not require the dissociation of N_2 as the first step involves the formation of NNH_2 (Figure 4) and its reduction to ammonia (Figure 11) is shown in Figure S9. The highest barriers on this compound pathway are **1.42** eV corresponding to TS5 of Figure 4, and 2.36 eV, corresponding to TS4-1 of Figure 11.

More compound pathways with higher barrier heights may be constructed with taking into consideration the pathways in Figure 3 and Figures S2, S3, and S4 from the Supporting Information. The pathway preference seems to depend on the local distributions of reagents and ambient conditions. Generally, the catalytic processes on the surface of an Fe_{16} catalyst leading to the formation of ammonia are more diverse than those on the bulk surfaces, and multiple mechanisms may be operational simultaneously.

This work, in which we have presented the mechanistic elucidation of the elementary reactions involved in the iron-catalyzed reduction of N_2 and H_2 to ammonia and the dependence of the reaction energetics on the total spin of the initial, final, and intermediate states, provides new insights relevant for the design and optimization of improved catalyst architectures for this extremely important reaction.

https://doi.org/10.1021/acs.jpca.3c05426
J. Phys. Chem. A 2023, 127, 9052−9068

■ ASSOCIATED CONTENT

Supporting Information

The Supporting Information is available free of charge at https://pubs.acs.org/doi/10.1021/acs.jpca.3c05426.

Potential energy curve for the $Fe_{16}N_2(2S + 1 = 51) + H_2(2S + 1 = 1)$ system (Figure S1), two pathways of an amino group are presented (Figures S2 and S3), the lowest energy isomers of $Fe_{16}N_2H_2$ (Figure S4), and a pathway of the NH_3 formation (Figure 5), four compound pathways discussed in the paper (Figures S6−S9), and Gaussian coordinates and total energies used for preparing Figures 2−16 and S2−S5 (PDF)

■ AUTHOR INFORMATION

Corresponding Author

Gennady L. Gutsev − *Department of Physics, Florida A&M University, Tallahassee, Florida 32307, United States;* orcid.org/0000-0001-7752-5567; Email: gennady.gutsev@famu.edu

Authors

Katharine M. Tibbetts − *Department of Chemistry, Virginia Commonwealth University, Richmond, Virginia 23284, United States;* orcid.org/0000-0001-8853-5656

Lavrenty G. Gutsev − *Federal Research Center of Problems of Chemical Physics and Medicinal Chemistry RAS, Chernogolovka 142432, Russia; Institute for Micromanufacturing, Louisiana Tech University, Ruston, Louisiana 71272, United States;* orcid.org/0000-0002-9679-9093

Sergey M. Aldoshin − *Federal Research Center of Problems of Chemical Physics and Medicinal Chemistry RAS, Chernogolovka 142432, Russia*

Bala R. Ramachandran − *Institute for Micromanufacturing, Louisiana Tech University, Ruston, Louisiana 71272, United States*

Complete contact information is available at: https://pubs.acs.org/10.1021/acs.jpca.3c05426

Notes

The authors declare no competing financial interest.

■ ACKNOWLEDGMENTS

Portions of this research were conducted with high-performance computational resources provided by the Louisiana Optical Network Infrastructure (http://www.loni.org). This research has also used resources of the National Energy Research Scientific Computing Center, a DOE Office of Science User Facility supported by the Office of Science of the U.S. Department of Energy under Contract No. DE-AC02-05CH11231. G.L.G. and K.M.T. acknowledge the support of the U.S. Army Research Office through Contract W911NF-19-1-0099. B.R.R. acknowledges the support from the National Science Foundation under Grant Number OIA-1946231. The work has been performed in accordance with the Russian Government state task (State Registration No. AAAA-A19-119111390022-2).

■ REFERENCES

(1) Lan, R.; Irvine, J. T.S.; Tao, S. Ammonia and Related Chemicals as Potential Indirect Hydrogen Storage Materials. *Int. J. Hydrogen Energy* **2012**, *37*, 1482−1494.

(2) MacFarlane, D. R.; Cherepanov, P. V.; Choi, J.; Suryanto, B. H. R.; Hodgetts, R. Y.; Bakker, J. M.; Ferrero Vallana, F. M.; Simonov, A. N. A Roadmap to the Ammonia Economy. *Joule* **2020**, *4*, 1186−1205.

(3) Liu, H. Ammonia synthesis catalyst 100 years: Practice, Enlightenment and Challenge. *Chin. J. Catal.* **2014**, *35*, 1619−1640.

(4) Foster, S. L.; Bakovic, S. I. P.; Duda, R. D.; Maheshwari, S.; Milton, R. D.; Minteer, S. D.; Janik, M. J.; Renner, J. N.; Greenlee, L. F. Catalysts for nitrogen reduction to ammonia. *Nat. Catal.* **2018**, *1*, 490−500.

(5) Ghavam, S.; Vahdati, M.; Wilson, A. G.; Styring, P. Sustainable Ammonia Production Processes. *Front. Energy Res.* **2021**, *9*, No. 580808.

(6) Howard, J. B.; Rees, D. C. Structural Basis of Biological Nitrogen Fixation. *Chem. Rev.* **1996**, *96*, 2965−2982.

(7) Howard, J. B.; Rees, D. C. How Many Metals Does It Take to Fix N_2? A Mechanistic Overview of Biological Nitrogen Fixation. *Proc. Natl. Acad. Sci. U.S.A.* **2006**, *103*, 17088−17093.

(8) Anderson, J. S.; Moret, M.-E.; Peters, J. C. Conversion of Fe−NH_2 to Fe−N_2 with release of NH_3. *J. Am. Chem. Soc.* **2013**, *135*, 534−537.

(9) Chalkley, M. J.; Drover, M. W.; Peters, J. C. Catalytic N2-to-NH3 (or -N2H4) Conversion by Well-Defined Molecular Coordination Complexes. *Chem. Rev.* **2020**, *120*, 5582−5636.

(10) Cui, X.; Tang, C.; Zhang, Q. A Review of Electrocatalytic Reduction of Dinitrogen to Ammonia under Ambient Conditions. *Adv. Energy Mater.* **2018**, *8*, No. 1800369.

(11) Suryanto, B. H. R.; Du, H.-L.; Wang, D.; Chen, J.; Simonov, A. N.; MacFarlane, D. R. Challenges and Prospects in the Catalysis of Electroreduction of Nitrogen to Ammonia. *Nat. Catal.* **2019**, *2*, 290−296.

(12) Shi, L.; Yin, Y.; Wang, S.; Sun, H. Rational Catalyst Design for N_2 Reduction under Ambient Conditions: Strategies toward Enhanced Conversion Efficiency. *ACS Catal.* **2020**, *10*, 6870−6899.

(13) Young, S. D.; Ceballos, B. M.; Banerjee, A.; Mukundan, R.; Pilania, G.; Goldsmith, B. R. Metal Oxynitrides for the Electrocatalytic Reduction of Nitrogen to Ammonia. *J. Phys. Chem. C* **2022**, *126*, 12980−12993.

(14) Li, P.; Fang, Z.; Jin, Z.; Yu, G. Ammonia Electrosynthesis on Single-Atom Catalysts: Mechanistic Understanding and Recent progress. *Chem. Phys. Rev.* **2021**, *2*, No. 041305.

(15) Zhang, S.; Zhao, Y.; Shi, R.; Waterhouse, G. I. N.; Zhang, T. Photocatalytic Ammonia Synthesis: Recent Progress and Future. *EnergyChem.* **2019**, *1*, No. 100013.

(16) Siegbahn, P. E. M.; Westerberg, J.; Svensson, M.; Crabtree, R. H. Nitrogen Fixation by Nitrogenases: A Quantum Chemical Study. *J. Phys. Chem. B* **1998**, *102*, 1615−1623.

(17) Lu, J.-B.; Ma, X.-L.; Wang, J.-Q.; Liu, J.-C.; Xiao, H.; Li, J. Efficient Nitrogen Fixation via a Redox-Flexible Single-Iron Site with Reverse-Dative Iron → Boron σ Bonding. *J. Phys. Chem. A* **2018**, *122*, 4530−4537.

(18) Li, X.-F.; Li, Q.-K.; Cheng, J.; Liu, L.; Yan, Q.; Wu, Y.; Zhang, X.-H.; Wang, Z.-Y.; Qiu, Q.; Luo, Y. Conversion of Dinitrogen to Ammonia by FeN_3-Embedded Graphene. *J. Am. Chem. Soc.* **2016**, *138*, 8706−8709.

(19) Zeinalipour-Yazdi, C. D.; Hargreaves, J. S. J.; Catlow, C. R. A. Low-T Mechanisms of Ammonia Synthesis on Co_3Mo_3N. *J. Phys. Chem. C* **2018**, *122*, 6078−6082.

(20) Ologunagba, D.; Kattel, S. Transition Metal Oxynitride Catalysts for Electrochemical Reduction of Nitrogen to Ammonia. *Mater. Adv.* **2021**, *2*, 1263−1270.

(21) Zeinalipour-Yazdi, C. D.; Hargreaves, J. S. J.; Laassiri, S.; Catlow, C. R. A. A Comparative Analysis of the Mechanisms of Ammonia Synthesis on Various Catalysts Using Density Functional Theory. *R. Soc. Open Sci.* **2021**, *8*, No. 210952.

(22) Geng, C.; Li, J.; Weiske, T.; Schwarz, H. Ta_2^+-Mediated Ammonia Synthesis from N_2 and H_2 at Ambient Temperature. *Proc. Natl. Acad. Sci. U.S.A.* **2018**, *115*, 11680−11687.

(23) Zhang, X.-L.; Ye, Y.-L.; Zhang, L.; Li, X.-H.; Yu, D.; Chen, J.-H.; Sun, W.-M. Designing an Alkali-Metal-Like Superatom Ca_3B for

Ambient Nitrogen Reduction to Ammonia. *Phys. Chem. Chem. Phys.* **2021**, *23*, 18908−18915.
(24) Cheng, R.; Cui, C.; Luo, Z. Catalysis of Dinitrogen Activation and Reduction by a Single Fe_{13} Cluster and its Doped Systems. *Phys. Chem. Chem. Phys.* **2023**, *25*, 1196−1204.
(25) Chen, B.; Gutsev, G. L.; Sun, W.; Kuang, X.; Lu, C.; Gutsev, L. G.; Aldoshin, S. M.; Ramachandran, B. R. Dissociation of Dinitrogen on Iron Clusters: A Detailed Study of the Fe_{16} + N_2 Case. *Phys. Chem. Chem. Phys.* **2021**, *23*, 2166−2178.
(26) Gutsev, G. L.; Tibbetts, K. M.; Gutsev, L. G.; Aldoshin, S. M.; Ramachandran, B. R. Mechanisms of Complete Dissociation of CO_2 on Iron Clusters. *ChemPhysChem* **2022**, *23*, No. e2022002.
(27) Perco, D.; Loi, F.; Bignardi, L.; Sbuelz, L.; Lacovig, P.; Tosi, E.; Lizzit, S.; Kartouzian, A.; Heiz, U.; Baraldi, A. The highest oxidation state observed in graphene-supported sub-nanometer iron oxide clusters. *Commun. Chem.* **2023**, *6*, 61.
(28) Gutsev, G. L.; Weatherford, C. A.; Jena, P.; Johnson, E.; Ramachandran, B. R. Structure and Properties of Fe_n, Fe_n^-, and Fe_n^+ clusters, n = 7−20. *J. Phys. Chem. A* **2012**, *116*, 10218−10228.
(29) Yuan, H. K.; Chen, H.; Kuang, A. L.; Tian, C. L.; Wang, J. Z. The Spin and Orbital Moment of Fe_n (n = 2−20) Clusters. *J. Chem. Phys.* **2013**, *139*, No. 034314.
(30) Kim, E.; Mohrland, A.; Weck, P. F.; Pang, T.; Czerwinski, K. R.; Tománek, D. Magic Numbers in Small Iron Clusters: A First-Principles Study. *Chem. Phys. Lett.* **2014**, *613*, 59−63.
(31) Frisch, M. J.; Trucks, G. W.; Schlegel, H. B.; Scuseria, G. E.; Robb, M. A.; Cheeseman, J. R.; Scalmani, G.; Barone, V.; Petersson, G. A.; Nakatsuji, H.; Li, X.; Caricato, M.; et al.*Gaussian 16*, Revision C.01; Gaussian, Inc.: Wallingford, CT, 2016.
(32) Becke, A. D. Density-Functional Exchange-Energy Approximation with Correct Asymptotic Behavior. *Phys. Rev. A* **1988**, *38*, 3098−3100.
(33) Perdew, J. P.; Wang, Y. Accurate and Simple Analytic Representation of the Electron-Gas Correlation Energy. *Phys. Rev. B* **1992**, *45*, 13244−13249.
(34) Curtiss, L. A.; McGrath, M. P.; Blaudeau, J.-P.; Davis, N. E.; Binning, R. C., Jr.; Radom, L. Extension of Gaussian-2 Theory to Molecules Containing Third-Row Atoms Ga−Kr. *J. Chem. Phys.* **1995**, *103*, 6104−6113.
(35) Frisch, M. J.; Pople, J. A.; Binkley, J. S. Self-Consistent Molecular Orbital Methods 25. Supplementary Functions for Gaussian Basis Sets. *J. Chem. Phys.* **1984**, *80*, 3265−3269.
(36) Li, S.; Dixon, D. A. Molecular Structures and Energetics of the $(TiO_2)_n$ (n = 1−4) Clusters and Their Anions. *J. Phys. Chem. A* **2008**, *112*, 6646−6666.
(37) Grein, F. Ground and Low-Lying Excited C_{2v} States of FeO_2 − A Challenge to Computational Methods. *Int. J. Quantum Chem.* **2009**, *109*, 549−558.
(38) Ju, M.; Lv, J.; Kuang, X.-Y.; Ding, L.-P.; Lu, C.; Wang, J.-J.; Jin, Y.-Y.; Maroulis, G. Systematic Theoretical Investigation of Geometries, Stabilities and Magnetic Properties of Iron Oxide Clusters $(FeO)_n^\mu$ (n = 1−8, μ = 0, ± 1): Insights and Perspectives. *RSC Adv.* **2015**, *5*, 6560−6570.
(39) Yang, K.; Zheng, J.; Zhao, Y.; Truhlar, D. G. Tests of the RPBE, revPBE, τ-HCTHhyb, ωB97X-D, and MOHLYP density functional approximations and 29 others against representative databases for diverse bond energies and barrier heights in catalysis. *J. Chem. Phys.* **2010**, *132*, No. 164117.
(40) Gutsev, G. L.; Aldoshin, S. M.; Gutsev, L. G.; Ramachandran, B. R. Evolution of Ferromagnetic and Antiferromagnetic States in Iron Nitride Clusters Fe_nN and Fe_nN_2 (n = 1−10). *J. Phys. Chem. A* **2021**, *125*, 7891−7899.
(41) Tan, L.; Liu, F.; Armentrout, P. B. Thermochemistry of the activation of N_2 on iron cluster cations: Guided ion beam studies of the reactions of Fe_n^+ (n = 1−19) with N_2. *J. Chem. Phys.* **2006**, *124*, No. 084302.
(42) Gutsev, G. L.; Belay, K. G.; Gutsev, L. G.; Ramachandran, B. R. Geometrical and Magnetic Structure of Iron Oxide Clusters $(FeO)_n$ for n > 10. *Comput. Mater. Sci.* **2017**, *137*, 134−143.
(43) Schlegel, H. B. Optimization of Equilibrium Geometries and Transition Structures. *J. Comput. Chem.* **1982**, *3*, 214−218.
(44) Fukui, K. The Path of Chemical Reactions — The IRC Approach. *Acc. Chem. Res.* **1981**, *14*, 363−368.
(45) Hratchian, H. P.; Schlegel, H. B. Accurate Reaction Paths Using a Hessian Based Predictor−Corrector Integrator. *J. Chem. Phys.* **2004**, *120*, 9918−9924.
(46) Niemeyer, M.; Hirsch, K.; Zamudio-Bayer, V.; Langenberg, A.; Vogel, M.; Kossick, M.; Ebrecht, C.; Egashira, K.; Terasaki, A.; Möller, T.; et al. Spin Coupling and Orbital Angular Momentum Quenching in Free Iron Clusters. *Phys. Rev. Lett.* **2012**, *108*, No. 057201.
(47) Adachi, S.; Kohguchi, H.; Suzuki, T. Unravelling the Electronic State of NO_2 Product in Ultrafast Photodissociation of Nitromethane. *J. Phys. Chem. Lett.* **2018**, *9*, 270−273.
(48) Garcia, J. M.; Shaffer, R. E.; Sayres, S. G. Ultrafast Pump-Probe Spectroscopy of Finite-Sized Neutral Iron Oxide Clusters. *Phys. Chem. Chem. Phys.* **2020**, *22*, 24624−24632.
(49) Kirilyuk, A.; Kimel, A. V.; Rasing, T. Ultrafast Optical Manipulation of Magnetic Order. *Rev. Mod. Phys.* **2010**, *82*, 2731−2784.
(50) Krieger, K.; Dewhurst, J. K.; Elliott, P.; Sharma, S.; Gross, E. K. U. Laser-Induced Demagnetization at Ultrashort Time Scales: Predictions of TDDFT. *J. Chem. Theory Comput.* **2015**, *11*, 4870−4874.
(51) Elliott, P.; Singh, N.; Krieger, K.; Gross, E. K. U.; Sharma, S.; Dewhurst, J. K. The microscopic origin of spin-orbit mediated spin-flips. *J. Magn. Magn. Mater.* **2020**, *502*, No. 166473.
(52) Zheng, Z.; Zheng, Q.; Zhao, J. Spin-orbit coupling induced demagnetization in Ni: *Ab initio* nonadiabatic molecular dynamics perspective. *Phys. Rev. B* **2022**, *105*, No. 085142.
(53) Glendening, E. D., Reed, A. E., Carpenter, J. E.; Weinhold, F. *NBO Version 3.1*.; Gaussian Inc.: Pittsburgh, PA, 2003.
(54) Burford, R. J.; Fryzuk, M. D. Examining the Relationship Between Coordination Mode and Reactivity of Dinitrogen. *Nat. Rev. Chem.* **2017**, *1*, 0026.
(55) Mou, L.-H.; Jiang, G.-D.; Li, Z.-Y.; He, S.-G. Activation of Dinitrogen by Gas-Phase Species. *Chin. J. Chem. Phys.* **2020**, *33*, 507−520.
(56) Straßner, A.; Wiehn, C.; Klein, M. P.; Fries, D. V.; Dillinger, S.; Mohrbach, J.; Prosenc, M. H.; Armentrout, P. B.; Niedner-Schatteburg, G. Cryo Spectroscopy of N_2 on Cationic Iron Clusters. *J. Chem. Phys.* **2021**, *155*, No. 244305.
(57) Straßner, A.; Klein, M. P.; Fries, D. V.; Wiehn, C.; Huber, M. E.; Mohrbach, J.; Dillinger, S.; Spelsberg, D.; Armentrout, P. B.; Niedner-Schatteburg, G. Kinetics of Stepwise Nitrogen Adsorption by Size-Selected Iron Cluster Cations: Evidence for Size-Dependent Nitrogen Phobia. *J. Chem. Phys.* **2021**, *155*, No. 244306.
(58) Ehrhard, A. A.; Klein, M. P.; Mohrbach, J.; Dillinger, S.; Niedner-Schatteburg, G. Cryo Kinetics of N_2 Adsorption onto Bimetallic Rhodium−Iron Clusters in Isolation. *J. Chem. Phys.* **2022**, *156*, No. 054308.
(59) Egeberg, R. C.; Dahl, S.; Logadottir, A.; Larsen, J. H.; Nørskov, J. H.; Chorkendorff, I. N_2 Dissociation on Fe(110) and Fe/Ru(0001): What is the Role of Steps? *Surf. Sci.* **2001**, *491*, 183−194.
(60) Ling, C.; Niu, X.; Li, Q.; Du, A.; Wang, J. Metal-Free Single Atom Catalyst for N_2 Fixation Driven by Visible Light. *J. Am. Chem. Soc.* **2018**, *140*, 14161−14168.
(61) Xu, L.; Kirvassilis, D.; Bai, Y.; Mavrikakis, M. Atomic and Molecular Adsorption on Fe(110). *Surf. Sci.* **2018**, *667*, 54−65.
(62) Liyanage, R.; Griffin, J. B.; Armentrout, P. B. Thermodynamics of Ammonia Activation by Iron Cluster Cations: Guided ion Beam Studies of the Reactions of Fe_n^+ (n = 2−10, 14) with ND_3. *J. Chem. Phys.* **2003**, *119*, 8979−8995.
(63) Armentrout, P. B. Chapter 6, Reactivity and Thermochemistry of Transition Metal Cluster Cations. In *Nanoclusters − a bridge across disciplines*; Jena, P., Castleman, A. W., Jr., Eds.; Science and Technology of Atomic, Molecular, Condensed Matter & Biological Systems; Elsevier: 2010; pp 269−297.

https://doi.org/10.1021/acs.jpca.3c05426
J. Phys. Chem. A 2023, 127, 9052−9068

(64) Parks, E. K.; Riley, S. J. Modeling Adsorbate Uptake: Coverage Dependence of the Iron Cluster-Ammonia Binding Energy. *J. Chem. Phys.* **1993**, *99*, 5898−5905.
(65) Jackson, K. A.; Knickelbein, M.; Koretsky, G.; Srinivas, S. The Interaction of Ammonia with Small Iron Clusters: Infrared Spectra and Density Functional Calculations of $Fe_n(NH_3)_m$ and $Fe_n(ND_3)_m$ complexes. *Chem. Phys.* **2000**, *262*, 41−51.
(66) Duan, X.; Ji, J.; Qian, G.; Fan, C.; Zhu, Y.; Zhou, X.; Chen, D.; Yuan, W. Ammonia Decomposition on Fe(110), Co(111) and Ni(111) surfaces: A density functional theory study. *J. Mol. Catal. A: Chem.* **2012**, *357*, 81−86.
(67) Ertl, G. Surface Science and Catalysis—Studies on the Mechanism of Ammonia Synthesis: The P. H. Emmett Award Address. *Catal. Rev. -Sci. Eng.* **1980**, *21*, 201−223.
(68) Ertl, G. Reactions at surfaces: from atoms to complexity (Nobel lecture). *Angew. Chem., Int. Ed.* **2008**, *47*, 3524−3535.

https://doi.org/10.1021/acs.jpca.3c05426
J. Phys. Chem. A 2023, 127, 9052−9068